ORIGINAL RESEARCH ARTICLE

Influence of Li_2O and Na_2O on Viscosity, Crystallization and Microstructure of High TiO_2-Containing Mold Slags

HEBIN JIN, XUEFENG XIE, SHENGPING HE, YATAO CUI, XUBIN ZHANG, and QIANGQIANG WANG

In the current study, the influence of Li_2O and Na_2O on the viscosity, crystallization, and structure of the high TiO_2-containing mold slag for the continuous casting of high-Ti steel was investigated to improve the property of the $CaO–SiO_2–TiO_2$-based slag under the steel-slag reaction through the measurement of the viscosity-temperature relationship, crystallization temperature and phases, and the Raman spectrum. With the increase of Li_2O content from 0 to 8 pct, the viscosity at 1300 °C and melting temperature decreased from 0.54 to 0.01 Pa s, and 1151 to 884 °C, respectively. While the viscosity of the slag at 1300 °C increased from 0.20 to 0.62 Pa s, the viscosity of the slag at 1400 °C decreased from 0.16 to 0.09 Pa s, and the melting temperature decreased from 1195 to 1077 °C with the Na_2O content from 2 to 10 pct. According to the thermodynamic calculation and XRD measurement, the main crystallization phase of high TiO_2 slags was $CaTiO_3$ with the content of Li_2O below 4 pct and Na_2O of 2 to 10 pct, the crystallization phase gradually changed from $CaTiO_3$ to $LiTiO_2$ with Li_2O from 4 to 8 pct, and the morphology of the crystalline nucleus changed from the type of spiky star to barbed sphere. Similarly, with the Li_2O content from 2 to 6 pct the initial and complete crystallization temperature decreased and increased, respectively, while those increased with the increase of Na_2O content, indicating that the increase of the Li_2O below 4 pct and the decrease of the Na_2O in the current slag resulted in the weak crystallization ability. With the addition of Li_2O content, the complex structural units of Q^1, Q^2 and Q^3 were depolymerized, and the slag viscosity decreased. With the increase of Na_2O content, structural units of Q^0, Q^1 and Q^2 structure units had the tendency to increase, and the viscosity of slag at 1400 °C decreased. These results could be used for the selection of typical components of mold slags for continuous casting of high-Ti steel.

https://doi.org/10.1007/s11663-024-03073-7

I. INTRODUCTION

HIGH Ti steel is characterized by high strength, good corrosion resistance, and excellent low-temperature performance. Nowadays, steel grades with the Ti content of 0.2 pct are often referred to as high-Ti steel,[1] which are widely used in automobiles, ships, bridges, aerospace, and other industries.[2,3] However, some problems often occur in continuous casting of high-Ti steel, such as the clogging of the submerged entry nozzle, the formation of floater at the steel-slag interface, and especially the steel-slag reaction ([Ti] + (SiO_2) = (TiO_2) + [Si]), which will result in the defect on the slab surface, and even the occurrence of breakout accident.[4–7] Under the steel-slag reaction, the composition of the mold slag gradually transforms from $CaO–SiO_2$ system to $CaO–TiO_2$ system, and the slag structure also changes from stable silicate to titanate, which in turn affects the properties of the slag. Hence, the use of non-reactive or low-reactive mold slag for the continuous casting of high-Ti steel is proposed by some researchers and scholars.

Numerous studies of the aforementioned issues have been reported. In consideration of the influence of the steel-slag reaction, TiO_2 was used as a substitute for SiO_2, and indicated that with TiO_2 addition the viscosity of the mold slag was decreased, Si–O and Al–O bond of the slag structure was depolymerized, and the slag

HEBIN JIN, XUEFENG XIE, SHENGPING HE, YATAO CUI, XUBIN ZHANG, and QIANGQIANG WANG are with the College of Materials Science and Engineering, and Chongqing Key Laboratory of Vanadium-Titanium Metallurgy and Advanced Materials, Chongqing University, Chongqiong 400044, P.R. China. Contact e-mail: zhangxubin12@163.com

Manuscript submitted January 10, 2024; accepted March 13, 2024. Article published online April 3, 2024.

polymerization was decreased.[8–10] However, when the TiO_2 content in the slag exceeds a certain limit, the performance of the slag with the precipitation of high melting temperature perovskite will deteriorate sharply.[11,12] The crystallization $CaTiO_3$ (or $CaO{\cdot}SiO_2{\cdot}TiO_2$, with high melting point) in mold slags has been made in previous studies as a function of TiO_2 addition.[13,14] Besides, TiO_2-containing mold slags have also been used to develop fluorine-free mold slags to control heat transfer by substituting perovskite for cuspidine.[15–21]

Previous studies have shown that the Li_2O and Na_2O can reduce the physicochemical properties of slag such as the viscosity and melting temperature. The increase of Li_2O in slags can reduce the viscosity and melting temperature of the mold slag, and provides free oxygen to simplify the silicate and aluminate ($[AlO_4]^-$ tetrahedral) network structure.[22–27] The addition of Li_2O (0 to 2 pct) decreases the crystallization ability of cuspidine with the lithium ions interfering with the interaction between Ca^{2+} ions and Li^+ ions, which retards the nucleation ability of cuspidine ($3CaO{\cdot}2SiO_2{\cdot}CaF_2$) and reduces the activity of SiO_2.[28,29] When the content of Li_2O exceeds a certain content, it will accelerate the precipitation of $LiAlO_2$ phase with high melting temperature.[30]

The influence of the Na_2O in different mold slag systems on the performance of mold slags is various. Li *et al.*[31] and Cui *et al.*[32] demonstrated that Na_2O reduced the viscosity of the slag, but resulted in the increase of slag crystallization. Wang *et al.*[29] found that viscosity decreased with the addition of Na_2O content from 0 to 10 pct in $CaO–Al_2O_3$-based mold slag. Wang *et al.*[33] investigated properties of $SiO_2–CaO–Al_2O_3–B_2O_3–Na_2O$ slags and found that the Na_2O content resulted in the increase of the break temperature and decrease of the viscosity. The relationship between the Na_2O and F contents and the crystallization of cuspidine was considered by Hanao *et al.*[34] through the X-ray diffraction analysis, and solidification temperatures of the mold flux at the $CaO–SiO_2–CaF_2–NaF$ system. Lu *et al.*[30] demonstrated that the increase of Li_2O and Na_2O in the $CaO–Al_2O_3–SiO_2$-based slag tend to inhibit crystallization. However, there have been few studies on the effect of Li_2O and Na_2O in $CaO–SiO_2–TiO_2$ slag system on the viscosity, crystallization and Raman structure properties of slag after the steel-slag reaction of high-Ti steel and slags. Therefore, it is necessary to study the influence of Li_2O and Na_2O content on basic properties of $CaO–SiO_2–TiO_2$-based slag.

In this study, slag systems with varying Li_2O and Na_2O contents were designed based on the mold slag with CaO/SiO_2 ratio of 0.93 as the original slag and with 12 pct TiO_2 content. The viscosity properties, melting properties, crystallization properties, and structure of mold slags were investigated using a rotational viscometer, melting temperature meter, improved high-temperature confocal equipment, X-ray diffraction (XRD), and Raman spectroscopy method.

II. EXPERIMENTAL METHODOLOGY

A. *Material Preparation*

In the current study, the influence of the Na_2O and Li_2O contents on the properties of the high TiO_2-containing mold slags after the steel-slag reaction is investigated, and the chemical compositions of mold slags are shown in Table I. These samples were prepared through the mixing and pre-melting of pure chemical reagent grade powders of $CaCO_3$, SiO_2, Al_2O_3, TiO_2, CaF_2, Na_2CO_3, $BaCO_3$, $MgCO_3$ and Li_2CO_3 at 1300 K, and then these homogeneous liquid slags were cooled as solid slags for the measurement of properties, respectively. During the continuous casting of mold slag of high titanium steel (825 Alloy, Ti = 0.9 pct) in a steel plant, the TiO_2 content in the liquid slag above the steel under the steel-slag reaction was approximately 12 pct, so the properties of two slags with the TiO_2 12 pct and SiO_2 28 pct were also discussed as L1 and N3. The content of the Li_2O and Na_2O was within 2~10 pct and 0~8 pct as L1~L5 and N1~N5, respectively.

B. *Measurement of Viscosity and Melting Temperature*

The viscosity at 1300 °C and viscosity-temperature relationship of mold slags are measured through the MTLQ-BQ-2 rotational viscometer, and the schematic of the viscometer is shown in Figure 1. The process of the viscosity measurement refers to the Chinese standard of mold slags (YB/T 185-2017). In order to ensure the uniform composition of slags, these slag samples (250 g)

Table I. Chemical Compositions of Mold Slags (Pct)

No.	CaO/SiO_2	CaO	SiO_2	Al_2O_3	TiO_2	CaF_2	Na_2O	BaO	MgO	Li_2O
L1	0.93	26	28	8	12	11	8	4	3	0
L2	0.93	25.1	26.9	8	12	11	8	4	3	2
L3	0.93	24.1	25.9	8	12	11	8	4	3	4
L4	0.93	23.1	24.9	8	12	11	8	4	3	6
L5	0.93	22.2	23.8	8	12	11	8	4	3	8
N1	0.93	28.9	31.1	8	12	11	2	4	3	0
N2	0.93	27.9	30.1	8	12	11	4	4	3	0
N3	0.93	27	29	8	12	11	6	4	3	0
N4	0.93	26	28	8	12	11	8	4	3	0
N5	0.93	25	27	8	12	11	10	4	3	0

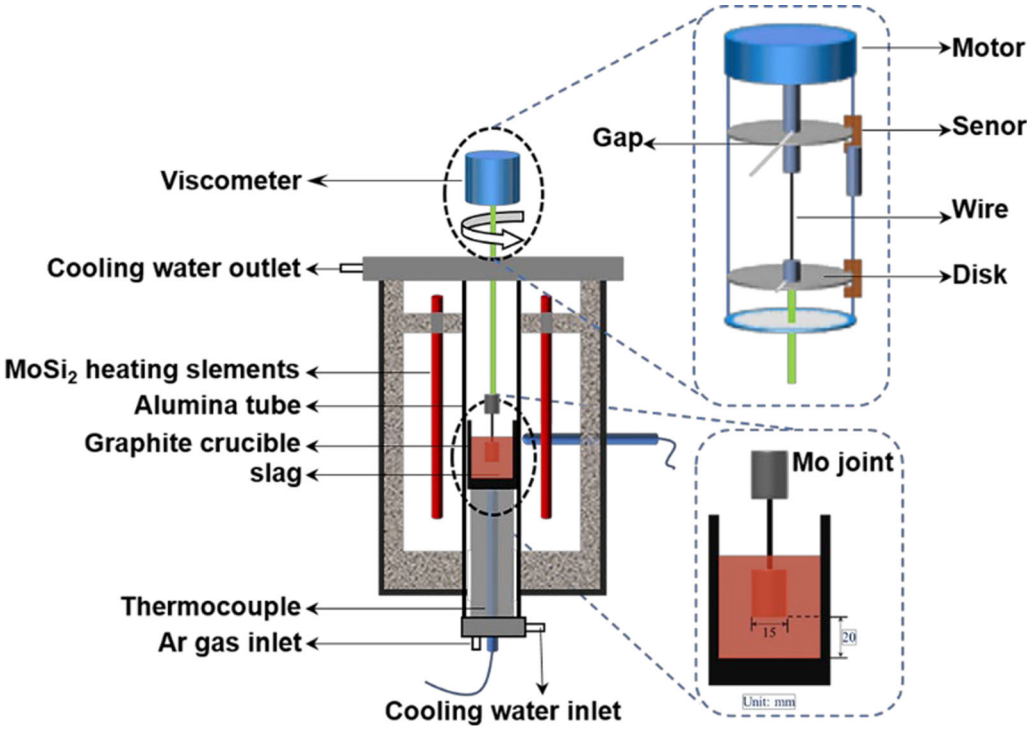

Fig. 1—Schematic setup for viscosity measurement.

were prepared, mixed, and then premelted in the high-temperature $MoSi_2$ furnace at 1300 °C at a rate of 15 °C/min for 30 minutes with these slags located in the graphite crucible. After the viscosity at 1300 °C was measured by the viscometer rotating at a fixed speed of 12 r/min, the viscosity-temperature relationship of the slag was recorded during the cooling process at the cooling rate of 6 °C/min until the viscosity exceeded 3.0 Pa s.[35]

The melting temperature of the mold slag composed of multi-components was not constant, and the hemisphere point temperature of the slag was considered as the melting temperature. After the viscosity measurement, the melting temperature (T_m) of the solid slag was measured through the hemisphere point method of the MTLQ-BQ-2 furnace. During the measurement of the melting temperature, the solid slag was crushed as powder, pressed as the cylinder with Φ3 mm × 3 mm, and then heated at the heating rate of 25 °C/min. The temperature with the height of the slag as half of the original one was considered as the melting temperature, and other details for the operation of the equipment could be found elsewhere.[36]

C. *Thermodynamic Calculation and Measurement of Slag Crystallization*

To understand the crystallization behavior of these mold slags, the thermodynamic calculation and experimental measurement were conducted through the FactSage 8.1 software and the modified full-field high-temperature confocal equipment, respectively. During the thermodynamic calculation based on the principle of minimum Gibbs Free Energy in equilibrium, the *Equilib* module was used, only the database of oxides and the product of the pure solid phase and all solution phases were chosen, and different precipitated phases within the temperature of 900 °C to 1500 °C were obtained and compared with different slag compositions in Table I. Besides, crystallization phases of mold slags were also detected by the XRD (X-Ray diffraction) (Model D/max 2500/PC Cu-Kα, Netherlands), and the sample for measurement was obtained through pouring the liquid slag into a cold stainless steel plate under the air cooling after liquid slags holding at 1300 °C or 800 °C.

During the measurement of the crystallization behavior including the observation of the crystallization process, and initial and complete crystallization temperature, about 75 mg of pre-melted solid samples were located into a platinum crucible, and then the crucible covered by a glass sheet to minimize the evaporation of fluoride was put into the modified confocal equipment for the crystallization measurement. Afterwards, the sample was heated to 1300 °C with a heating rate of 20 °C/min, kept for 90 seconds, and then cooled at different cooling rates of 0.2 or 1~4 °C/s. During the cooling of the sample, the crystallization process of mold slags was observed and recorded by camera,[37] and the initial and complete crystallization temperature and average crystallization rate were obtained.

D. *Measurement of Structural Units Through Raman Spectrum*

To explain the variation of the viscosity-temperature relationship and crystallization behavior of different mold slags, the structural units in molten slags were measured by the Raman spectrum. At first, the

premelted liquid slag at 1300 °C was quenched in cold water to obtain the amorphous sample, dried, and then ground to 200 mesh for XRD measurement. Without crystal in the quenched slag, the slag was used for the measurement of structural units through the Raman spectrum (LabRAM HR Evolution; HORIBA Jobin Yvon S.A.S., France) with a spectral range of 200 to 1600 cm^{-1}. The content of each structural unit in the slag was calculated by Peakfit software by the Gaussian function, and the influence of Li_2O and Na_2O on the degree of polymerization of slags was obtained.

III. VISCOSITY AND MELTING PROPERTIES

In the continuous casting of steel, the viscosity of slags was directly related to the lubrication of the slag on the solidified shell, and also the slag consumption, while the melting temperature affected the melting rate of slag powder, the thickness of the liquid slag pool and the length of the liquid slag film from the meniscus to the mold exit.

The viscosity-temperature relationship with different contents of Li_2O and Na_2O in slags is shown in Figure 2, and the viscosity at 1300 °C or 1400 °C and melting temperature of different Li_2O and Na_2O contents are compared in Figure 3. From Figure 2, the viscosity-temperature curve tended to move towards the high-viscosity region with increasing Li_2O content from 0 to 8 pct and Na_2O content from 2 to 10 pct, respectively. From Figs. 2 and 3, the viscosity of the slag at 1300 °C decreased from 0.54 to 0.01 Pa s, and increased from 0.20 to 0.62 Pa s with the Li_2O and Na_2O content from 0 to 8 pct and 2 to 10 pct, respectively. With the increasing Na_2O content at 1400 °C, the viscosity of the slag decreased from 0.16 to 0.09 Pa s. The melting temperature greatly decreased from 1151 to 884 °C and 1195 to 1077 °C with the Li_2O and Na_2O content from 0 to 8 pct and 2 to 10 pct, respectively. The increase of the TiO_2 at the content of 12 pct in the slag under the steel-slag reaction would deteriorate the lubrication on the solidified shell, while the increase of the Li_2O in the TiO_2-containing slag could improve the lubrication, which is consistent with previous research.[25,36,38–44]

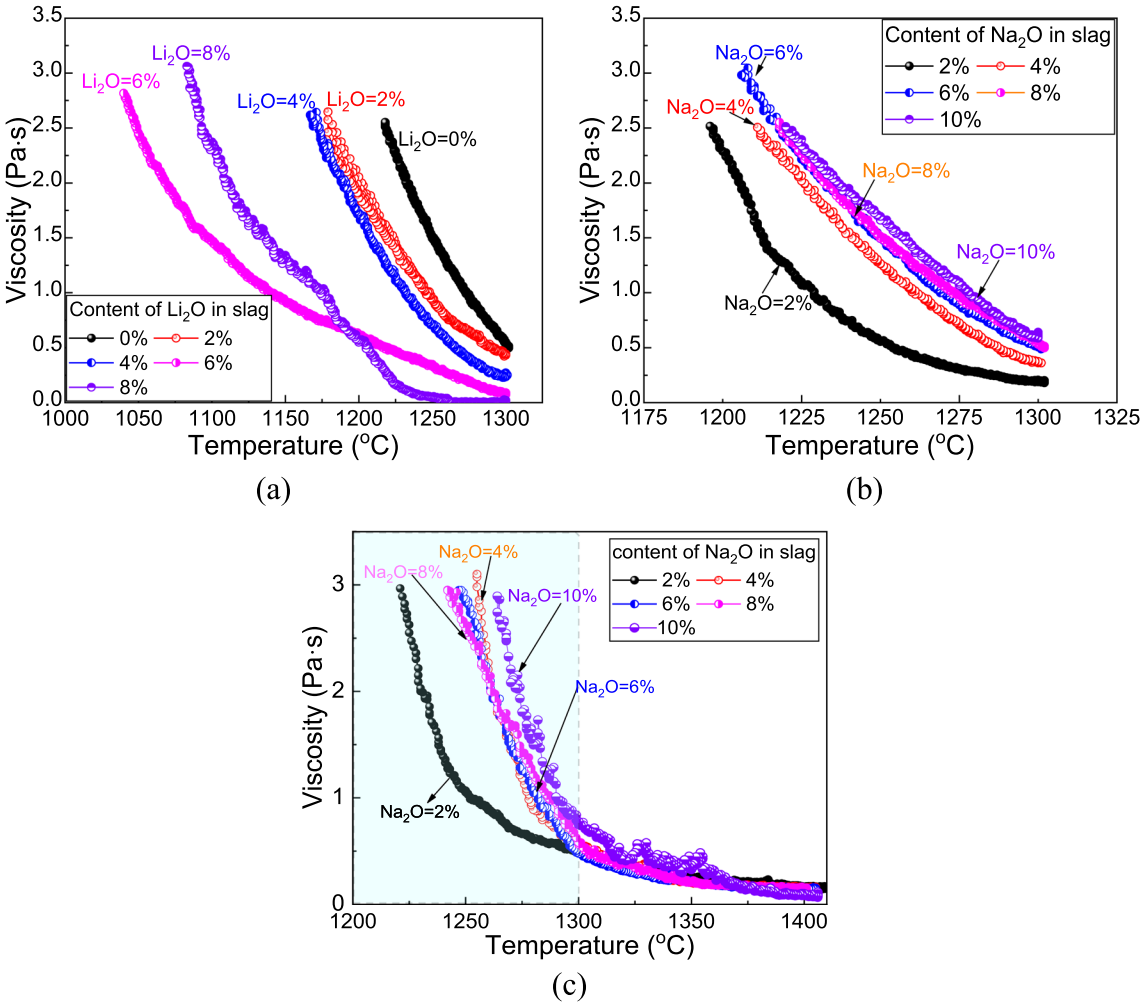

Fig. 2—Viscosity-temperature curves of mold slags with (*a*) the Li_2O content of 0~8 pct and (*b*) the Na_2O content of 0~10 pct at 1300 °C (*c*) the Na_2O content of 0~10 pct at 1400 °C.

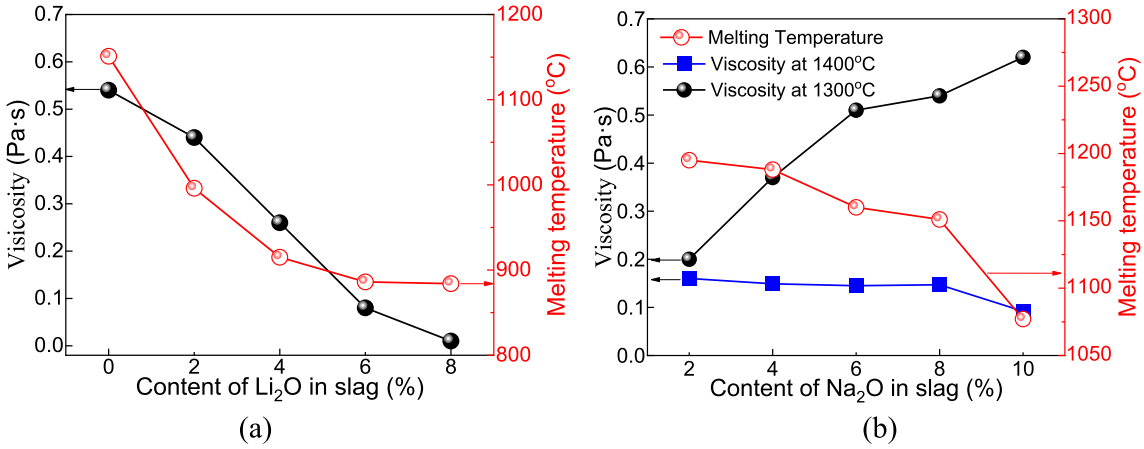

Fig. 3—Viscosity at 1300 °C or 1400 °C and melting temperature of mold slags with different (*a*) Li_2O and (*b*) Na_2O contents.

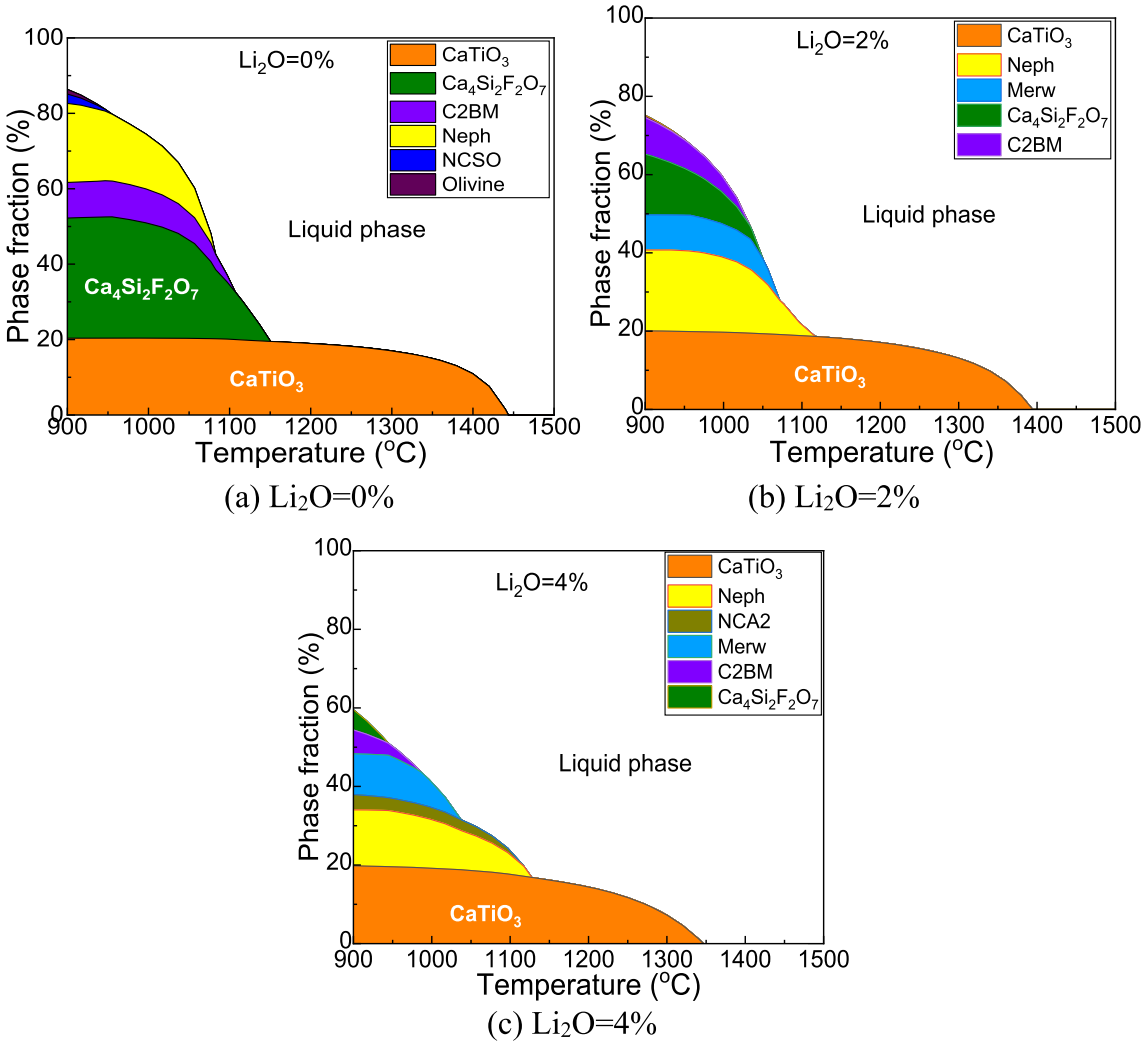

Fig. 4—Thermodynamic calculation of crystallization phases of mold slags with the Li_2O content of (*a*) 0 pct, (*b*) 2 pct and (*c*) 4 pct.

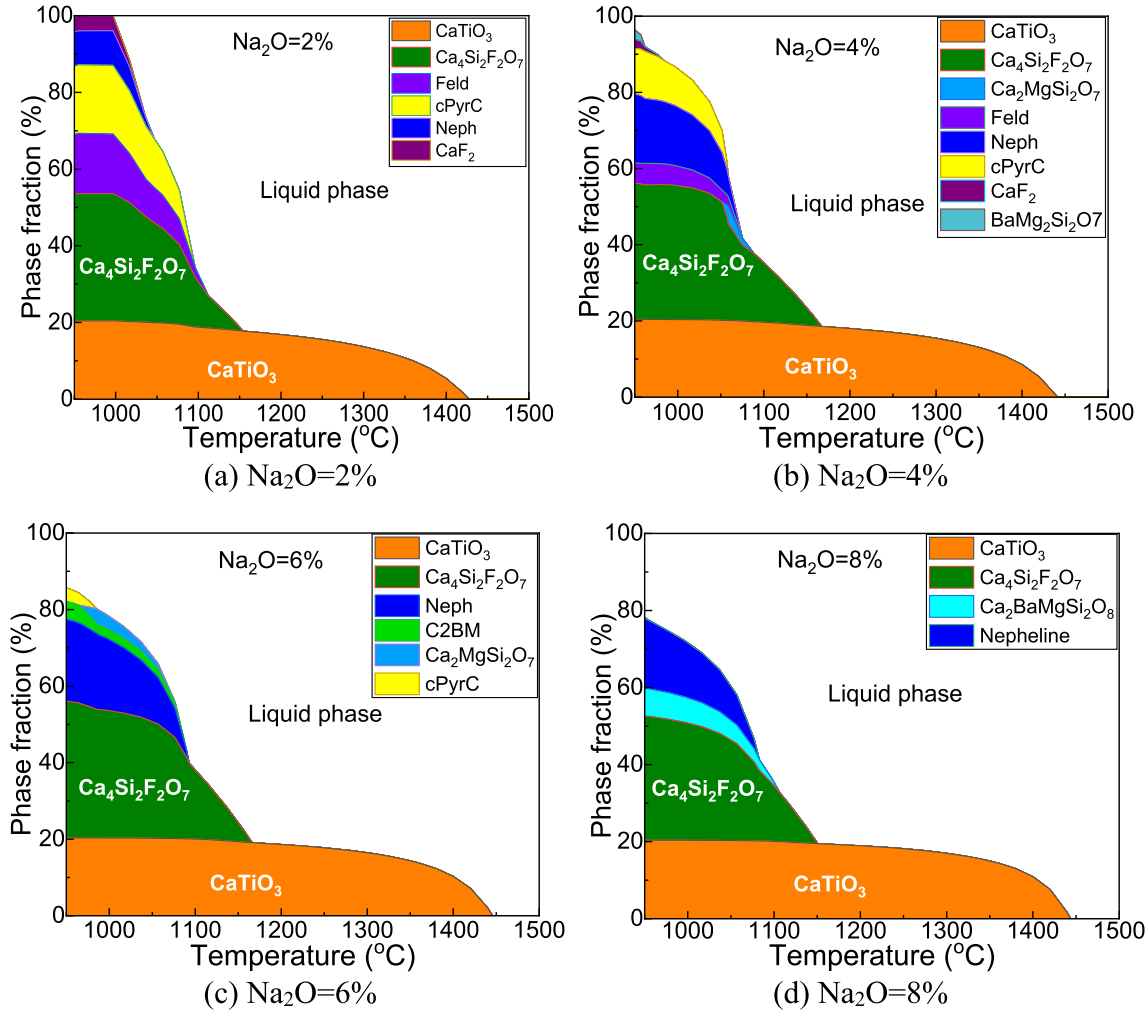

Fig. 5—Thermodynamic calculation of crystallization phases of mold slags with the Na_2O content of (*a*) 2 pct, (*b*) 4 pct, (*c*) 6 pct and (*d*) 8 pct.

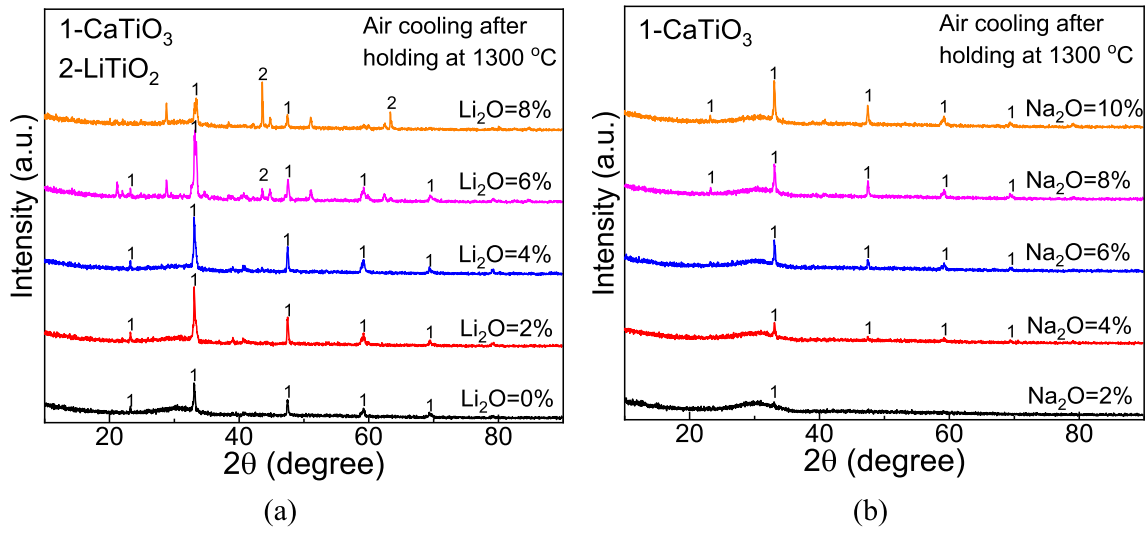

Fig. 6—Crystallization phases of mold slags with different (*a*) Li_2O and (*b*) Na_2O contents under air cooling after holding at 1300 °C.

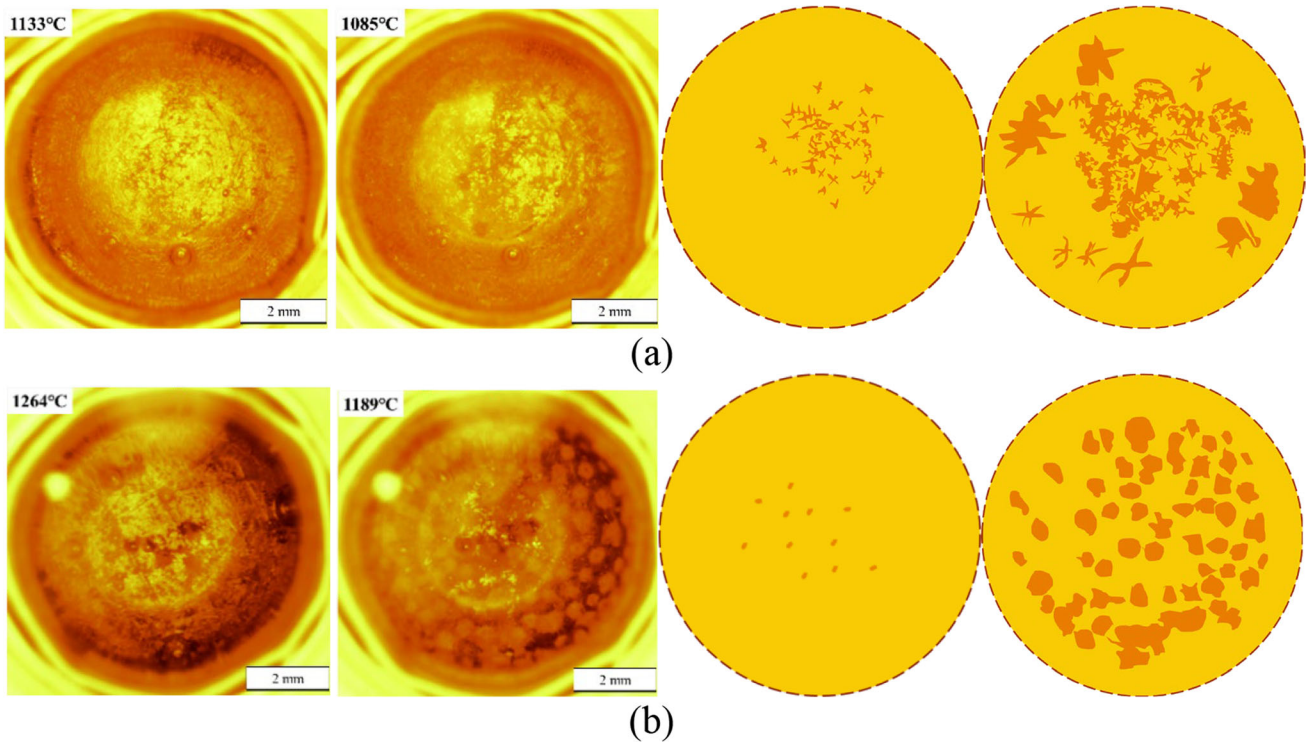

Fig. 7—Crystallization behavior of mold slags with the Li_2O content of (*a*) 2 pct and (*b*) 6 pct.

However, the viscosity increased with an increase in Na_2O content from 2 to 10 pct at 1300 °C (Figure 2(b)), which was different from the results of the previous studies.[38–40,43] In this study, the viscosity-temperature curves were further investigated at 1400 °C based on the results mentioned above. The results revealed that Na_2O, an alkali oxide, still had the function of reducing the viscosity at high-temperature (at 1400 °C). The viscosity of the slag corresponding to the temperature at 1300 °C is close to the break temperature. In the $CaO–SiO_2–TiO_2$ mold slag system, the increase of Na_2O content enhances the $CaTiO_3$ crystallization ability, which leads to an increase in viscosity with the increasing Na_2O content at 1300 °C. This indicates that the precipitation of crystals and the complex ions cluster structure will affect the increase of the viscosity of the slag (in Figure 2(c)).

IV. CRYSTALLIZATION BEHAVIOR AND PHASES

A. *Crystallization Phases Through Thermodynamic Calculation*

In Figures 4 and 5, the precipitated phase fraction of several mold slags with different temperature is also shown through the thermodynamic calculation of slags with the Li_2O of 0 to 4 pct and Na_2O of 2 to 8 pct. The thermodynamic calculation of phase precipitation could not be conducted with excessive Li_2O or Na_2O in slags, which was related to the data deficiency of these slags. From Figures 4 and 5, with the TiO_2 content of 12 pct in slags, the initial precipitated phase was perovskite ($CaTiO_3$) as the major phase with different Li_2O and Na_2O contents, and the second precipitated phase changed from cuspidine ($Ca_4Si_2F_2O_7$) to Neph ($NaAlSiO_4$) with the Li_2O from 0 to 4 pct, while that all was the cuspidine ($Ca_4Si_2F_2O_7$) phase with was Na_2O of 2 to 8 pct. From Figure 4, with the increase of the Li_2O in slags from 0 to 4 pct, the initial precipitated temperature of perovskite decreased from 1440 to 1340 °C, while that slightly increased from 1420 to 1440 °C with Na_2O from 0 to 8 pct in Figure 5. Hence, according to the thermodynamic calculation, the increase of Li_2O within 0 to 4 pct and the decrease of Na_2O content could result in the decrease of the crystallization ability in the high TiO_2-containing slag.

B. *Crystallization Phases Through XRD*

In Figure 6, crystallization phases through the XRD method are compared with different Li_2O and Na_2O contents under air cooling after holding at 1300 °C. With Li_2O of 0 to 4 pct and Na_2O of 2 to 10 pct under the air cooling after holding at 1300 °C, respectively. From Figure 6(a), with the increase of Li_2O from 0 to 8 pct, the crystallization phase gradually changed from perovskite ($CaTiO_3$) to $LiTiO_2$, and the phase of $LiTiO_2$ existed as the major phase. From Figure 6(b), with the increase of Na_2O from 0 to 10 pct, the intensity of the perovskite diffraction peak gradually enhanced, and the increase of Na_2O in slags promoted the precipitation of

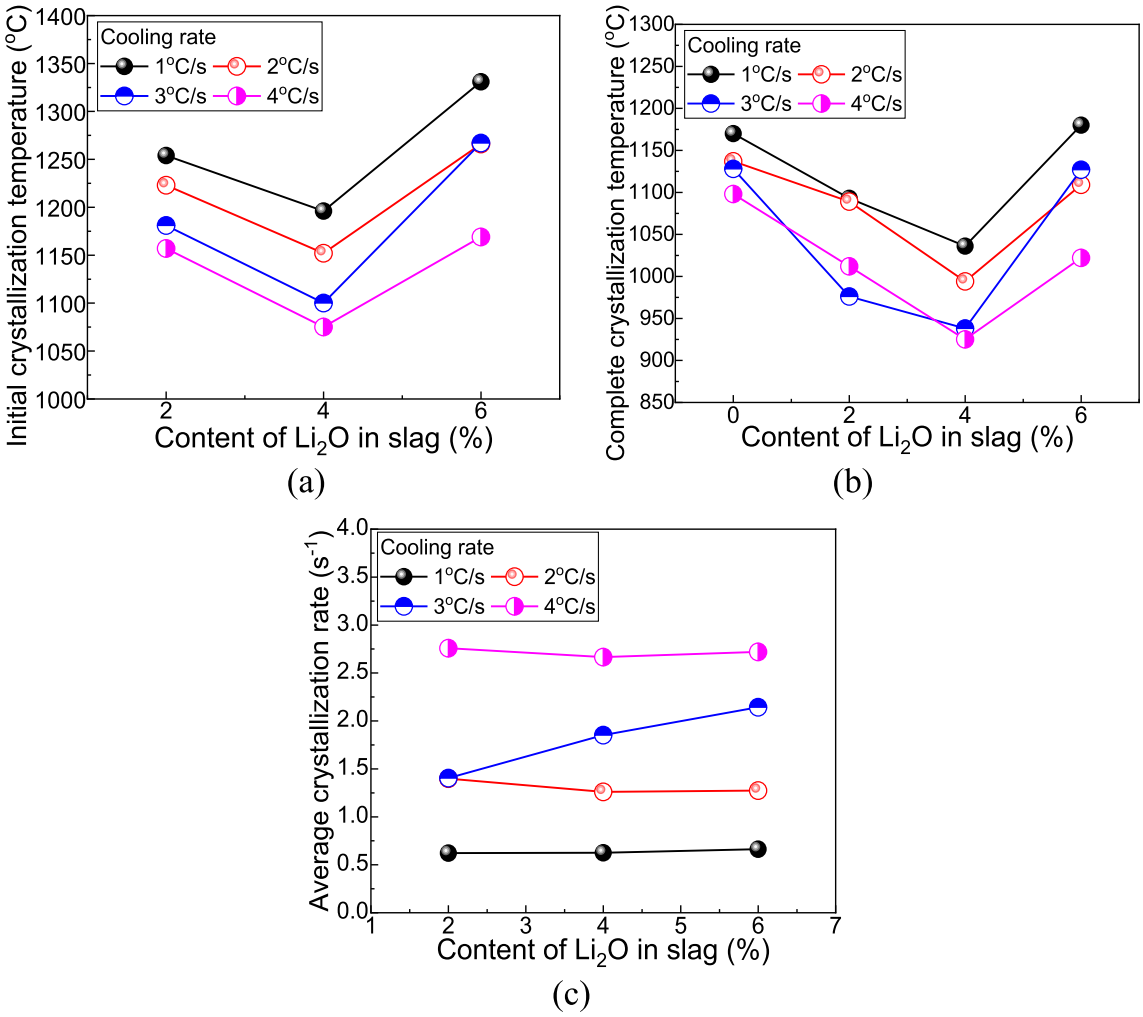

Fig. 8—(*a*) Initial crystallization temperature, (*b*) complete crystallization temperature and (*c*) average crystallization rate of mold slags with the Li_2O content of 2~6 pct.

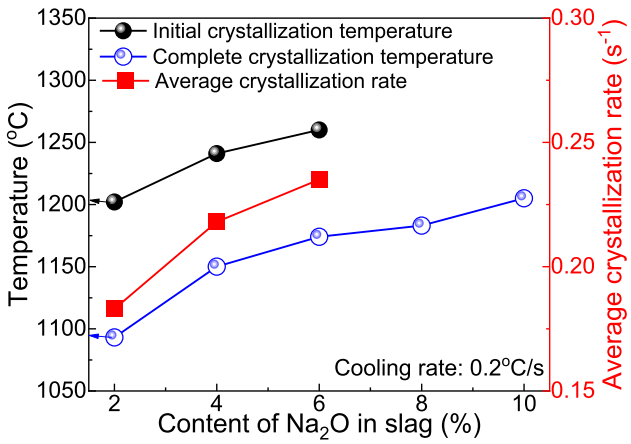

Fig. 9—Initial and complete crystallization temperature, and average crystallization rate of mold slags with different Na_2O contents of 2~10 pct.

$CaTiO_3$, and enhanced the crystallization ability of the high TiO_2 containing mold slags. It has been demonstrated that with an increase in Na_2O content in the slag, the precipitation of high melting point perovskite increased, and the break temperature increased, which ultimately resulted in a trend of increasing slag viscosity at 1300 °C.

C. *Crystallization Behavior and Temperature*

The crystallization behavior of mold slags with Li_2O of 2 and 6 pct is compared in Figure 7, and the initial crystallization temperature, complete crystallization temperature and average crystallization rate are shown in Figure 8 with different cooling rates and Li_2O contents. From Figures 6 and 7, with the Li_2O content from 2 to 6 pct, the crystallization phase gradually changed from $CaTiO_3$ to $LiTiO_2$, and the morphology of the crystalline nucleus changed from the type of spiky star to barbed sphere, which would affect the crystallization ability of slags. With 12 pct TiO_2 in slags, the crystallization ability was strong, so the cooling rate of the measurement was chosen as 1 to 4 °C/s. The initial crystallization temperature of slags with Li_2O of 0 and 8 pct was above 1350 °C, which was not measured. From Figure 8, with the increase of the Li_2O from 0 to

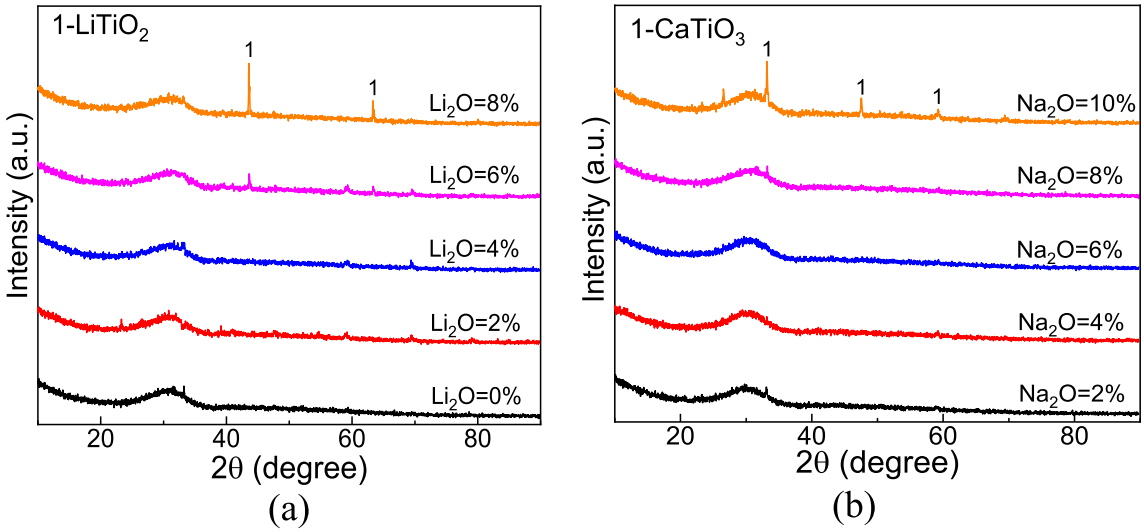

Fig. 10—XRD results of these mold slags under the water cooling.

Table II. Correspondence Between Raman Shift and Structural Units

Raman Shift (cm^{-1})	Structure Unit	References
550	Al–O–Al	[45–49]
659~676	O–Si–O	[9]
722~738	O–Ti–O	[50, 51]
750~800	$Al–O^-$ (monomer)	[13, 27, 51–53]
850~880	Q^0 ($[SiO_4^{4-}]$ monomer), or Ti–O–Ti (Ti–O–Si) structural groups	[54–57]
900~930	Q^1 ($[Si_2O_7^{6-}]$ polyhedra)	[54, 55]
940~980	Q^2 ($[Si_2O_6^{4-}]$ chain)	[56, 57]
1010~1040	Q^3 ($[Si_2O_5^{2-}]$ sheet)	[58–60]

6 pct at different cooling rates, the initial crystallization temperature and the complete crystallization temperature of these slags decreased and then increased, while the average crystallization rate changed less, indicating that the transition of crystallization phase from $CaTiO_3$ to $LiTiO_2$ increased the overall crystallization temperature, but the difference of crystallization rate of these two phases was small. With the increase of the cooling rate from 1 to 4 °C/s, the initial and complete crystallization temperature decreased, while the average crystallization rate increased from ~ 0.6 to ~ 2.7 s^{-1}, indicating that large supercooling promoted the growth of crystals in current slags. Hence, with the increase of Li_2O from 0 to 4 pct, the crystallization ability of these high TiO_2-containing slags decreased, while that greatly increased with the Li_2O from 4 to 8 pct and the increase of the cooling rate.

In Figure 9, the initial crystallization temperature, complete crystallization temperature and the average crystallization rate are compared with different Na_2O contents in slags at the cooling rate of 0.2 °C/s. In current slags, the crystallization ability was weak with low Na_2O content, and the crystallization process of the mold slag cannot be observed with the high cooling rate of 1~4 °C/s, so the cooling rate of 0.2 °C/s was selected for the study of different Na_2O mold slag. From Figure 9, with the increase of Na_2O content from 2 to 6 pct, the initial and the average crystallization temperature of mold slags increased from 1202 °C to 1260 °C and 0.18 to 0.23 s^{-1}, respectively, while the complete crystallization temperature increased from 1093 °C to 1205 °C with the Na_2O from 2 to 10 pct. The variation of initial crystallization temperature of the perovskite ($CaTiO_3$) through thermodynamic calculation in Figure 5 and measurement in Figure 6(b) had the same tendency. Hence, the increase of Na_2O in current slags promoted crystallization ability through the increase of the crystallization temperature and rate.

V. STRUCTURE OF MOLD SLAGS THROUGH RAMAN SPECTRUM

A. *Crystallization of Water-Quenched Samples*

The XRD crystal phase analysis results of the water-quenched samples are shown in Figure 10. The obvious characteristic peaks of $LiTiO_2$ and $CaTiO_3$ appeared in the spectrum, when the Li_2O content reached 6 pct, and Na_2O content reached 8 pct.

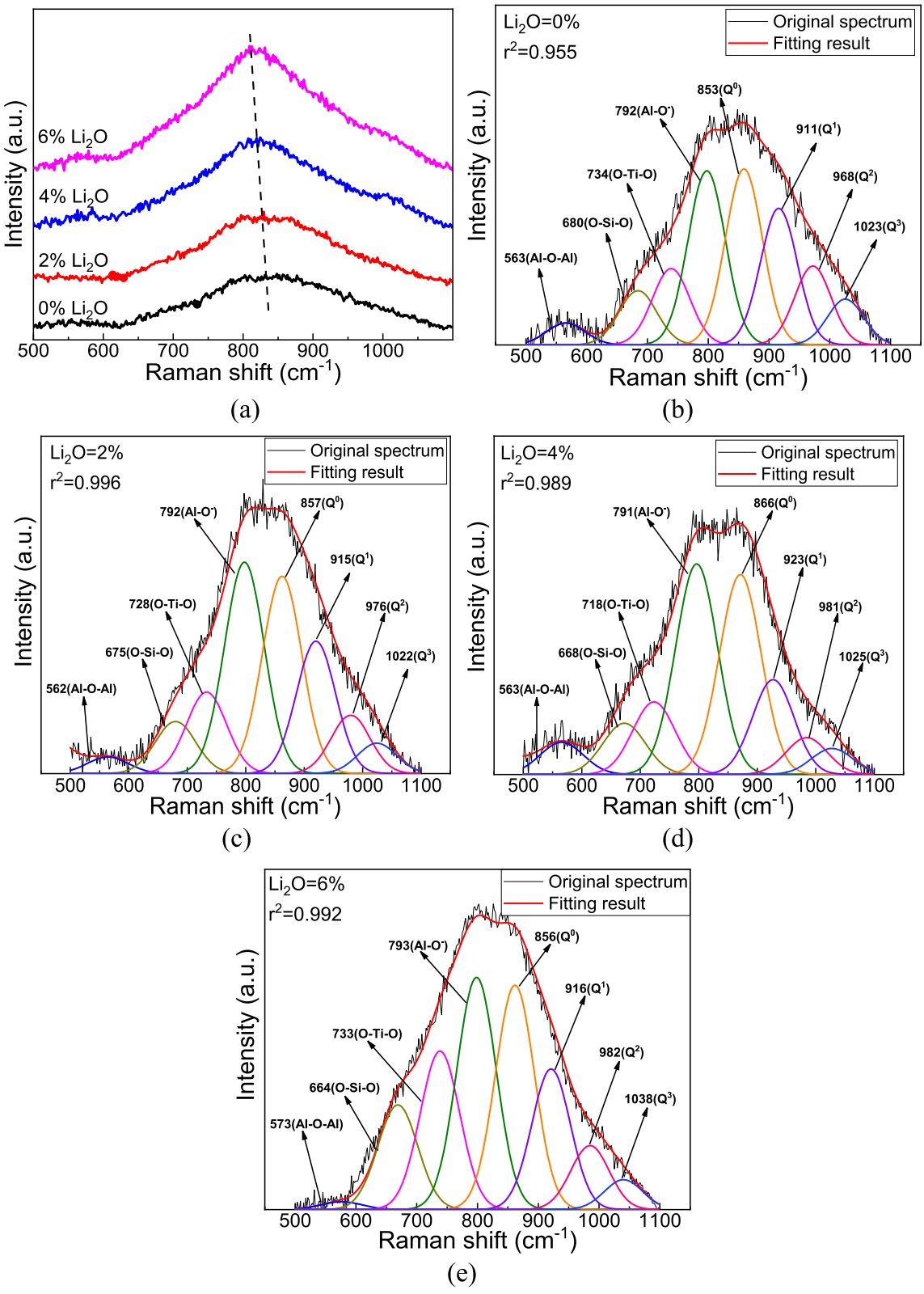

Fig. 11—Peak fitting results of Raman spectrum of mold slag with different Li_2O content.

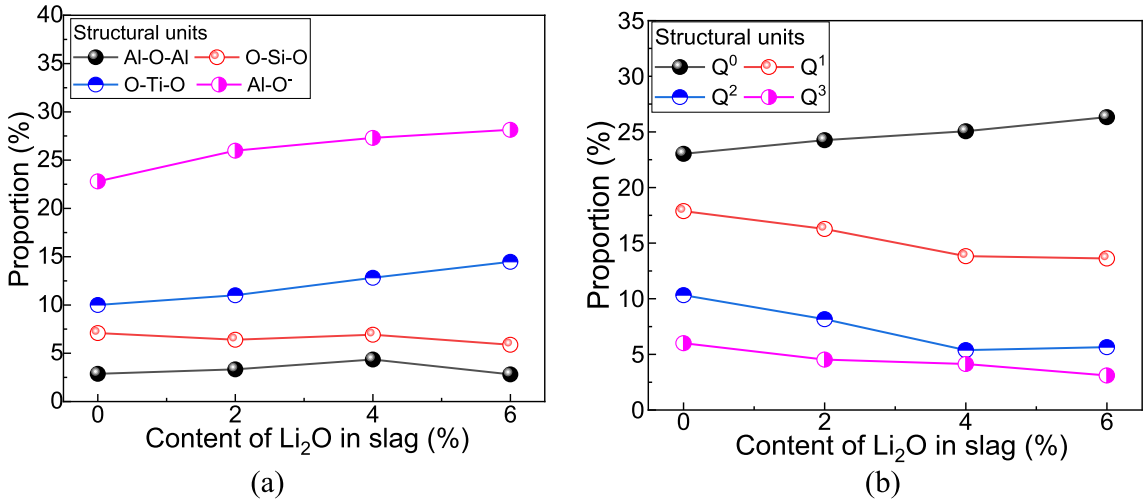

Fig. 12—Structural units proportion of mold slag with different Li_2O content.

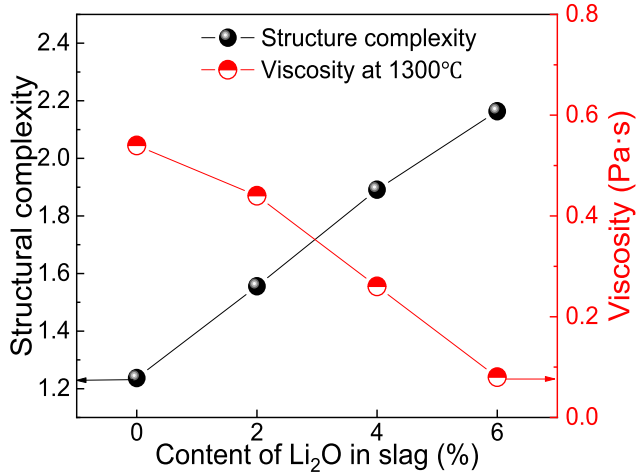

Fig. 13—Viscosity and structure complexity with varying content of Li_2O in slag.

Water-cooled slag structure was performed using Raman spectroscopy to determine the effect of component changes. The impact of a small amount of crystallization on the slag structure was considered in the result analysis.

B. *Structural Units of Mold Slags with Different Li_2O and Na_2O Contents*

Different displacements correspond to the expansion and deformation vibration of different structural units, and the corresponding relationship is shown in Table II. Area fractions of various bands in the middle frequency of 500 to 1100 cm^{-1} could be calculated from deconvolved spectra data.

The Gaussian deconvolution of the Raman spectrum and peak fitting results in the mold slags are shown in Figure 11 of different Li_2O, for which all Raman spectra are successfully fitted at the frequency range of 500 to 1100 cm^{-1}. The main peak of the Raman spectrum curve was located near 830 cm^{-1}, and the highest peak was slightly red-shift to the low-frequency region with the increased Li_2O content. The width of the main peak gradually decreased, and the structural units in the slag were more concentrated near the peak. Figures 11(b), (c), (d), (e) shows that, with the addition of Li_2O from 0 to 6 pct, the tensile vibration of the simple structural units $Al–O^-$ and Q^0 (Ti–O–Ti or Ti–O–Si) gradually increased in the region of 750 to 880 cm^{-1}. Due to the high SiO_2 content, the slag is primarily composed of silicate structure, only a small portion of the titanoaluminate structure. The fractions of Q^1, Q^2 and Q^3 units in the silicate zone gradually decreased in the region of 900 to 1100 cm^{-1}. The Ca^{2+}, Ba^{2+}, Na^+, and Li^+ ions enriched in the negatively charged $Al–O^-$ tetrahedra provide charge compensation in the vicinity of the tetrahedra to charge balance, and provide O^{2-} ions to be used to depolymerize the bridged-oxygen network bonds.[61,62] It means that the increase in Li_2O content changes the complex network structure into simple silicate and titanium-aluminate monomers, the slag polymerization decreases and the structure becomes simpler.

The structural unit proportion of the mold slags at different Li_2O contents are statistically analyzed in Figure 12. As can be seen from Figures 12(a) and (b), with the addition of Li_2O, the Al–O–Al and O–Si–O structure units remained stable, the O–Ti–O, $Al–O^-$ and Q^0 structure units exhibited an increasing trend, the Q^1, Q^2 and Q^3 structure units showed a decreasing trend. This implies that some depolymerizations between Q^1, Q^2 and Q^3 complex structure units occur. It is proposed that Li_2O behaved as a network modifier in the molten slag,[28,29] and the dissociation of O^{2-} ions depolymerized the complex network structure, generating more non-bridging oxygen. The ratio of simple structures unit ($Al–O^- + Q^0$) and complex structures unit ($Al–O–Al + Q^1 + Q^2 + Q^3$) can be utilized to characterize the

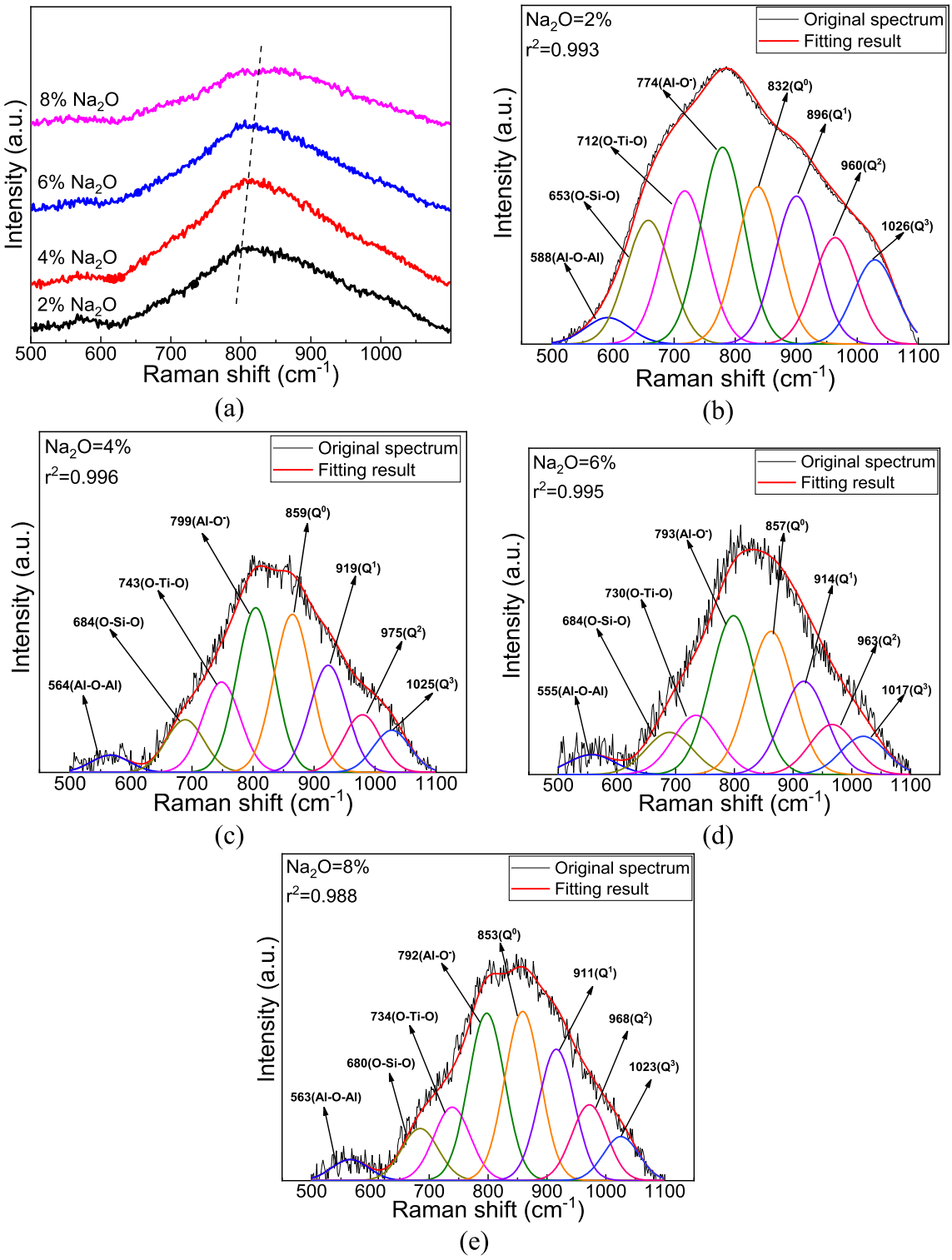

Fig. 14—Peak fitting results of Raman spectrum of mold slag with different Na_2O content.

structural complexity of the containing TiO_2 slag. Figure 13 shows viscosity and structural complexity with the addition of Li_2O in slag. The structure complexity decreases with the increasing Li_2O content. Consequently, the structure of the slag was simplified and the viscosity of the mold slag was reduced.

C. *Structural Units of Mold Slags with Different Na_2O Contents*

The effects of different Na_2O on the Raman spectroscopy and fitting results of the mold slag are shown in Figure 14, for which all Raman spectra are successfully fitted at the frequency range of 500 to 1100 cm^{-1}. There

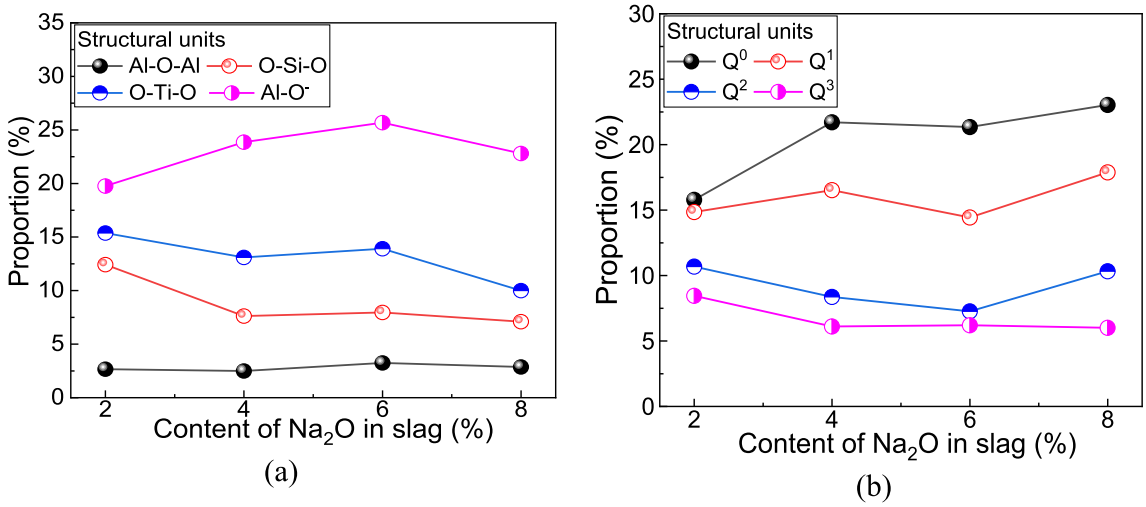

Fig. 15—Structural unit proportion of mold slag with different Na_2O content.

was only one peak near 810 cm^{-1} in Raman spectra. The position of the highest peak moved slightly blue-shift to the high-frequency region and the intensity of the peak was higher and the width was narrower with the addition of Na_2O content from 2 to 6 pct. Figures 14(b), (c), (d), and (e) shows that, with the addition of Na_2O, the tensile vibration of the simple structural units $Al–O^-$ and Q^0 gradually decreased in the region of 750 to 880 cm^{-1}. The fractions of Q^1, Q^2 and Q^3 units in the silicate zone gradually become stronger in the region of 900 to 1100 cm^{-1}. Furthermore, the wave peaks began to move towards the high-frequency region, the width increased, and the distribution of structural units became more dispersed.

In Figure 15, the structural units proportion of the mold slag at different Na_2O contents are statistically analyzed. Based on Figures 15(a) and (b), with the addition of Na_2O from 2 to 6 pct, the Al–O–Al structure units remained stable, the O–Si–O, O–Ti–O and Q^3 structure units decreased slowly, and the Q^0 and Q^1 structural units maintain growth trend; the $Al–O^-$ structural units had a tendency to increase and then decrease, whereas the Q^2 structural units exhibit the opposite trend. When Na_2O exceeds 6 pct, $Al–O^-$ structure began to decrease, Q^1 and Q^2 begin to increase, the O–Ti–O bond also decreases, and the structure of slag becomes more complex. The ratio of simple structures unit ($Al–O^- + Q^0$) to complex structures unit ($Al–O–Al + Q^1 + Q^2 + Q^3$) can be used a measure of the structural complexity of the slag. This means that Na_2O can decrease the degree of polymerization of the slag and the viscosity of the mold slag was decreased (at 1400 °C). Figure 16 show viscosity and structural complexity with the addition of Na_2O in slag. When the Na_2O content exceeds 8 pct, the crystallization ability of the slag is increased, and the precipitated microcrystals will affect the structural distribution of the slag. At a temperature of 1300 °C, the slag crystallization ability affects its viscosity. Therefore, the dotted area of structural complexity in Figure 16 shows a

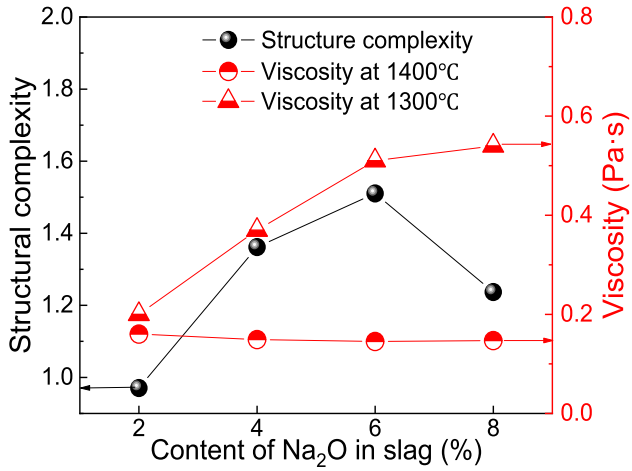

Fig. 16—Viscosity and structure complexity with varying content of Na_2O in slag.

downward trend. As a result, there is an opposite relationship between the viscosity of slag at 1300 °C and 1400 °C.

VI. CONCLUSIONS

The effects of different contents of Li_2O and Na_2O on physicochemical properties of the $CaO–SiO_2$-based mold slags for casting high-Ti steels were critically assessed. The basic properties such as T_m and viscosity of high-Ti steel mold slag were tested by rotary viscometer and hemisphere point method. The crystallization properties of mold slag, such as crystallization thermodynamics, crystallization phase and crystallization temperature, were studied using FactSage 8.1 software, modified full-field high-temperature confocal microscope, and XRD. The effects of typical components on the microstructure characteristics of the melt were analyzed by Raman spectroscopy. The conclusions are as follows:

1. With increasing Li_2O content, the viscosity and T_m of mold slag at 1300 °C decreased from 0.54 to 0.01 Pa s, and from 1151 °C to 884 °C, respectively. With increasing Na_2O content, the viscosity at 1300 °C increased from 0.20 to 0.62 Pa s, while the viscosity at 1400 °C decreased from 0.16 to 0.09 Pa s, and T_m decreased from 1195 °C to 1077 °C. It means that the addition of Na_2O enhances the crystallization ability of the mold slag and thus influences the trend of slag viscosity at 1300 °C.
2. The first precipitated perovskite ($CaTiO_3$) phase and the crystallization temperature of mold slag decreased gradually with the increase of Li_2O content (0 to 4 pct). The first precipitated temperature of perovskite ($CaTiO_3$) increased, and the precipitated cuspidine ($Ca_4Si_2F_2O_7$) phase decreased, with the increase of Na_2O (2 to 8 pct). XRD results shown that the crystalline mineral phase in the slag was transformed into $LiTiO_2$ as Li_2O content was 6 pct, and the crystallization temperature of the slag increased. Na_2O was the opposite. When the Li_2O content was constant, the initial crystallization temperature gradually decreased, the average crystallization rate increased, and the morphology of the crystalline nucleus changed from the type of spiky star to barbed sphere with the Li_2O increased from 2 to 6 pct. With the increase of Na_2O content from 2 to 6 pct, the initial and the average crystallization temperature of mold slags increased at the cooling rate of 0.2 °C/s.
3. With increasing Li_2O content, the Al–O–Al and O–Si–O structure units remained stable, the O–Ti–O, $Al–O^-$ and Q^0 structure units exhibited an increasing trend, and the complex structural units of Q^1, Q^2 and Q^3 were depolymerization. The total polymerization degree and viscosity of the slag decreased. With the addition of Na_2O from 2 to 6 pct, the Q^0 and Q^1 structural units maintain growth trend; the $Al–O^-$ structural units had a tendency to increase and then decrease, whereas the Q^2 structural units decrease and then increase, and the structure of slag (at 1400 °C) becomes more simpler.

ACKNOWLEDGMENTS

The authors are grateful for support from the Fundamental Research Funds for the Central Universities (Grant No. 2023CDJXY-020), the National Natural Science Foundation China (Grant Nos. 52074054, 52374325, 52004045), the postdoctoral research funding from Chongqing, College of Materials Science and Engineering at Chongqing University, China, and the Henan Tongyu Metallurgy Materials Group Co. Ltd., Xixia, China.

CONFLICT OF INTEREST

No conflict of interest exits in the submission of this manuscript, and manuscript is approved by all authors for publication. I would like to declare on behalf of my coauthors that the work described was original research that has not been published previously, and not under consideration for publication elsewhere, in whole or in part.

REFERENCES

1. Z. Chen: *Theoretical Research and Application of Continuous Casting Mold Fluxes for High Ti-bearing Alloy Steel*, Chongqing University, Chongqing, 2019.
2. F. Xie, W. Chen, Y. Wang, and D. Ma: *Heat Treat. Met.*, 2016, vol. 41, pp. 100–04.
3. Z. Liu, H. Wang, J. Li, X. Wang, and J. Deng: *Hebei Metall.*, 2011, vol. 8, pp. 27–30.
4. Z. Chen, M. Li, X. Wang, S. He, and Q. Wang: *Metals*, 2019, vol. 9, p. 635.
5. H. Todoroki, T. Ishii, K. Mizuno, and A. Hongo: *Mater. Sci. Eng. A*, 2005, vol. 413–414, pp. 121–28.
6. J.A. Bothma and P.C. Pistorius: *Ironmak. Steelmak.*, 2007, vol. 34, pp. 513–20.
7. Z. Chen, K. Xu, S. He, Q. Wang: In *Proceedings of the 8th International Symposium on High-Temperature Metallurgical Processing*, San Diego, 26 February–2 March 2017, pp. 169–76.
8. Z. Wang, Q. Shu, X. Hou, and K. Chou: *Ironmak. Steelmak.*, 2013, vol. 39, pp. 210–15.
9. Z. Wang, Q. Shu, and K. Chou: *Metall. Mater. Trans. B*, 2013, vol. 44B, pp. 606–13.
10. J. Ji, Y. Cui, S. Wang, S. He, Q. Wang, and X. Zhang: *Ceram. Int.*, 2022, vol. 48, pp. 256–326.
11. T. Mukongo, P.C. Pistorius, and A.M. Garbers-Craig: *Ironmak. Steelmak.*, 2004, vol. 31, pp. 135–43.
12. G. Wen, S. Sridhar, P. Tang, X. Qi, and Y. Liu: *ISIJ Int.*, 2007, vol. 47, pp. 1117–25.
13. J. Li, Q. Shu, X. Hou, and K. Chou: *ISIJ Int.*, 2014, vol. 55, pp. 830–36.
14. W. Yan, Z. Hao, W. Chen, and J. Li: *J. Mater. Res. Technol.*, 2021, vol. 10, pp. 882–94.
15. J. Yang, J. Zhang, Y. Sasaki, O. Ostrovski, and Y. Kashiwaya: *ISIJ Int.*, 2016, vol. 56, pp. 574–83.
16. Z. Wang, Q. Shu, and K. Chou: *Can. Metall. Quart.*, 2013, vol. 52, pp. 405–12.
17. Z. Wang, Q. Shu, and K. Chou: *Steel Res. Int.*, 2013, vol. 84, pp. 766–76.
18. J. Klug, R. Hagemann, N.C. Heck, A.C.F. Vilela, H.P. Heller, and P.R. Scheller: *Steel Res. Int.*, 2012, vol. 83, pp. 1186–93.
19. Q. Xin, G. Wen, and P. Tang: *J. Iron Steel Res.*, 2010, vol. 17, pp. 6–10.
20. Z. Zhang, J. Li, and P. Liu: *J. Iron. Steel Res. Int.*, 2011, vol. 18, pp. 31–37.
21. H. Nakada and K. Nagata: *ISIJ Int.*, 2006, vol. 46, pp. 441–49.
22. Q. Wang, J. Yang, J. Zhang, O. Ostrovski, C. Zhang, and D. Cai: *Steel Res. Int.*, 2021, vol. 93, p. 2100193.
23. G. Kim and I. Sohn: *ISIJ Int.*, 2011, vol. 51, pp. 1–8.
24. G. Kim and I. Sohn: *ISIJ Int.*, 2012, vol. 52, pp. 68–73.
25. J. Qi, C. Liu, and M. Jiang: *J. Non-Cryst. Solids*, 2017, vol. 475, pp. 101–07.
26. W. Wang, X. Yan, L. Zhou, S. Xie, and D. Huang: *Metall. Mater. Trans. B*, 2016, vol. 47B, pp. 963–73.
27. L. Zhou, H. Li, W. Wang, D. Xiao, L. Zhang, and J. Yu: *Metall. Mater. Trans. B*, 2018, vol. 49B, pp. 2232–40.
28. S. He, Q. Wang, X. Dan, C. Xu, Z. Li, and K.C. Mills: *Int. J. Min. Met. Mater.*, 2009, vol. 16, pp. 261–64.
29. W. Wang, H. Shao, L. Zhou, H. Luo, and H. Wu: *Ceram. Int.*, 2020, vol. 46, pp. 26880–87.
30. B. Lu, K. Chen, W. Wang, and B. Jiang: *Metall. Mater. Trans. B*, 2014, vol. 45B, pp. 1496–1509.
31. J. Li, W. Wang, J. Wei, D. Huang, and H. Matsuura: *ISIJ Int.*, 2012, vol. 52, pp. 2220–25.
32. Y. Cui, H. Fan, Z. Guo, G. Wang, X. Li, J. Zhao, and Z. Yang: *J. Iron. Steel Res. Int.*, 2019, vol. 26, pp. 412–21.

33. L. Wang, C. Zhang, D. Cai, and J. Zhang: *Metall. Mater. Trans. B*, 2017, vol. 48B, pp. 516–26.
34. M. Hanao, M. Kawamoto, and T. Watanabe: *ISIJ Int*., 2004, vol. 44, pp. 827–35.
35. T. Wu, Q. Wu, S. He, J. Xu, and Y. Lu: *Steel Res. Int*., 2012, vol. 83, pp. 1194–1202.
36. L. Zhu, Q. Wang, Q. Wang, S. Zhang, and S. He: *J. Am. Ceram. Soc*., 2019, vol. 102, pp. 104–08.
37. X. Yan, W. Pan, X. Wang, X. Zhang, and Q. Wang: *Metall. Mater. Trans. B*, 2021, vol. 52B, pp. 2526–35.
38. Z. Pang, X. Xing, Q. Xue, J. Wang, and H. Zuo: *Ceram. Int*., 2022, vol. 48, pp. 23357–64.
39. X. Zhang, C. Liu, and M. Jiang: *Metall. Mater. Trans. B*, 2021, vol. 52B, pp. 2604–11.
40. J.B. Kim and I. Sohn: *ISIJ Int*., 2014, vol. 54, pp. 2050–058.
41. C. Shi, S. Shin, D. Zheng, J. Cho, and J. Li: *Metall. Mater. Trans. B*, 2016, vol. 47B, pp. 3343–49.
42. H.S. Park, H. Kim, and I. Sohn: *Metall. Mater. Trans. B*, 2011, vol. 42B, pp. 324–30.
43. Z. Chang, K. Jiao, X. Ning, and J. Zhang: *Metall. Mater. Trans. B*, 2019, vol. 50B, pp. 1399–406.
44. J. Gao, G. Wen, Q. Sun, P. Tang, and Q. Liu: *Metall. Mater. Trans. B*, 2015, vol. 46B, pp. 1850–59.
45. P. Mcmillan, B. Piriou, and A. Navrotsky: *Geochim. Cosmochim. Acc*., 1982, vol. 46, pp. 2021–37.
46. E. Gao, W. Wang, and L. Zhang: *J. Non-Crystal. Solids*, 2017, vol. 473, pp. 79–86.
47. Y. Sun, W. Hao, and Z. Zhang: *Metall. Mater. Trans. B*, 2018, vol. 49B, pp. 677–87.
48. I. Daniel, P. Gillet, P.F. Mcmillan, and B.T. Poe: *Phys. Chem. Miner*., 1995, vol. 22, pp. 74–86.
49. J. Li, Q. Shu, and K. Chou: *Can. Metall. Quart*., 2015, vol. 54, pp. 85–91.
50. B. Mysen and D. Neuville: *Geochim. Cosmochim. Acta*, 1995, vol. 59, pp. 325–42.
51. B. Mysen, F. Ryerson, and D. Virgo: *Am. Mineral*., 1980, vol. 65, pp. 1150–65.
52. Z. Yan, X. Lv, Z. Pang, X. Lv, and C. Bai: *Metall. Mater. Trans. B*, 2018, vol. 49B, pp. 1322–30.
53. D. Liang, Z. Yan, X. Lv, J. Zhang, and C. Bai: *Metall. Mater. Trans. B*, 2017, vol. 48B, pp. 573–81.
54. B. Mysen, D. Virgo, and C. Scarfe: *Am. Mineral*., 1980, vol. 65, pp. 690–710.
55. B. Mysen, L. Finger, V. David, and F. Seifert: *Am. Mineral*., 1982, vol. 67, pp. 686–95.
56. B. Mysen, D. Virgo, and F. Seifert: *Rev. Geophy*., 1982, vol. 20, pp. 353–83.
57. L. Hwa, S. Hwang, and L. Liu: *J. Non-Crystal. Solids*, 1998, vol. 238, pp. 193–97.
58. J. Li, Y. Sun, Z. Li, and Z. Zhang: *ISIJ Int*., 2016, vol. 56, pp. 752–58.
59. R. Akagi, N. Ohtori, and N. Umesaki: *J. Non-Crystal. Solids*, 2001, vol. 293, pp. 471–76.
60. J. Tan, S. Zhao, W. Wang, G. Davies, and X. Mo: *Mat. Sci. Eng. B*, 2004, vol. 106, pp. 295–99.
61. T.S. Kim and J.H. Park: *ISIJ Int*., 2014, vol. 54, pp. 2031–38.
62. Z. Wang, Q. Shu, and K. Chou: *High Temp. Mat. Pr-ISR*., 2011, vol. 30, pp. 233–39.